

Accumulation mode field-effect transistors for improved sensitivity in nanowire-based biosensors

David J. Baek, Juan P. Duarte, Dong-Il Moon, Chang-Hoon Kim, Jae-Hyuk Ahn et al.

Citation: *Appl. Phys. Lett.* **100**, 213703 (2012); doi: 10.1063/1.4723843

View online: <http://dx.doi.org/10.1063/1.4723843>

View Table of Contents: <http://apl.aip.org/resource/1/APPLAB/v100/i21>

Published by the [American Institute of Physics](http://www.aip.org).

Related Articles

Molecular-scale bio-sensing using armchair graphene

J. Appl. Phys. **112**, 014905 (2012)

Nanofluidic preconcentration and detection of nanoparticles

J. Appl. Phys. **112**, 014304 (2012)

Biofunctionalized AlGaIn/GaN high electron mobility transistor for DNA hybridization detection

Appl. Phys. Lett. **100**, 232109 (2012)

Polymer translocation under time-dependent driving forces: Resonant activation induced by attractive polymer-pore interactions

JCP: BioChem. Phys. **6**, 05B620 (2012)

Polymer translocation under time-dependent driving forces: Resonant activation induced by attractive polymer-pore interactions

J. Chem. Phys. **136**, 205104 (2012)

Additional information on *Appl. Phys. Lett.*

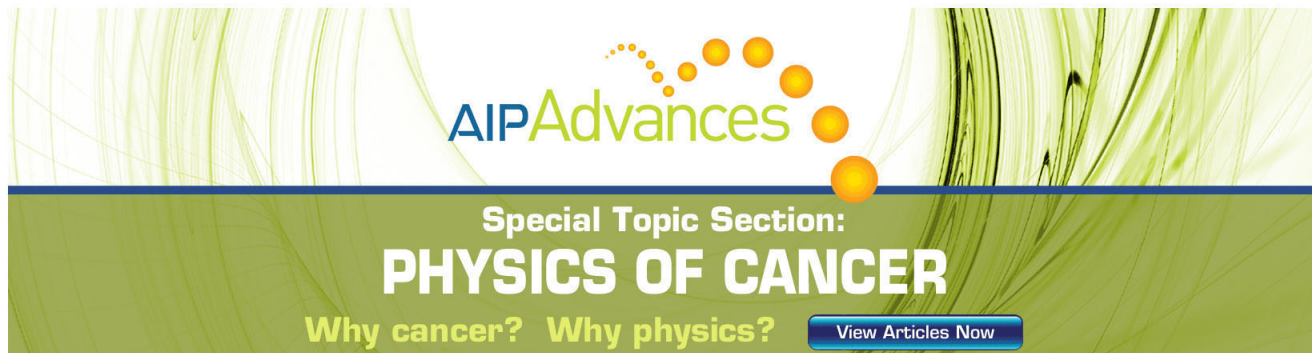
Journal Homepage: <http://apl.aip.org/>

Journal Information: http://apl.aip.org/about/about_the_journal

Top downloads: http://apl.aip.org/features/most_downloaded

Information for Authors: <http://apl.aip.org/authors>

ADVERTISEMENT



AIP Advances

Special Topic Section:
PHYSICS OF CANCER

Why cancer? Why physics? [View Articles Now](#)

Accumulation mode field-effect transistors for improved sensitivity in nanowire-based biosensors

David J. Baek, Juan P. Duarte, Dong-II Moon, Chang-Hoon Kim, Jae-Hyuk Ahn, and Yang-Kyu Choi^{a)}

Department of Electrical Engineering, KAIST, Daejeon 305-701, South Korea

(Received 30 April 2012; accepted 11 May 2012; published online 25 May 2012)

In this work, nanowire field-effect transistors (NW-FETs) constructed from a top-down approach has been utilized for the detection of biomolecules. Here, we demonstrate that the sensitivity of NW-FET sensors can be greatly enhanced when the same dopant type is used for both channel region and source and drain. This type of FET, known as accumulation mode field-effect transistors (AM-FETs), functions under different operating principle compared with conventional inversion mode FETs. The improved sensitivity is attributed to the different conduction mechanism and current components of AM devices. The results have been verified through a direct comparison with a conventional FET. © 2012 American Institute of Physics. [<http://dx.doi.org/10.1063/1.4723843>]

Owing to their comparable sizes to biomolecules, semiconductor nanowires (NWs) have attracted substantial interests from the scientific community for their application as sensors.¹⁻⁶ Among the semiconductor NWs, silicon nanowire field-effect transistors (SiNW-FETs) are currently under intense research due to their high reproducibility, well-understood material surface chemistry, and compatibility with the CMOS technology.⁷⁻¹⁰ Up till now, various approaches have been undertaken to find different ways to better the sensitivity of SiNW-FET sensors. These efforts include studying the dependence of device sensitivity on the NW dimensions,¹¹⁻¹³ influence of doping concentration,^{1,14} and comparison of the subthreshold regime and the linear regime for the optimal sensitivity.¹⁵ Due to the well-established silicon technology and the well-understood physics behind semiconductors, above approaches indicate further room for improvement. In this work, we suggest that by employing accumulation mode field-effect transistors (AM-FETs), which operate under different principles compared with conventional inversion mode field-effect transistors (IM-FETs), the device sensitivity can be improved significantly.

Recently, Colinge *et al.* reported a new type of transistor, i.e., junctionless field-effect transistors (FETs), in which there is no junctions.¹⁶ In this rather unorthodox transistor, the dopant atoms and their doping concentration within the device are same across the channel region and source and drain (S/D). AM-FETs, which is the type employed in this work, can be regarded as junctionless FETs with lower channel doping concentration.^{16,17} That is, while the doping across junctionless devices is $N^+-N^+-N^+$, that across AM devices is $N^+-N^+-N^+$. As both types of transistors consist of channels that have the same polarity as the semiconductor region in which they are formed on, the operating principles and thus the conduction mechanism are similar. For conventional IM-FETs, devices are turned on as inversion channel is formed near the surface. Hence, the carriers only travel within the confined inversion layer and thus the main con-

duction mechanism is through surface current. However, when the dopant atoms are of the same type across the whole device, which is the case for junctionless FETs and AM-FETs, the relative energy barrier between the channel region and S/D is already small without the presence of any gate voltage (V_G) applied. In other words, the device contains neutral silicon in which carriers can flow through the nanowire with only the drain-source voltage (V_{DS}) applied.^{18,19} Therefore, in this case, as the formation of a channel is unnecessary, carriers are not confined to a specific path and are able to flow through the whole bulk region.¹⁶⁻¹⁹ Still, when sufficient V_G is applied, channel is subsequently formed in the surface area and surface current begins to flow in addition to the bulk current. In our approach, this fundamental difference has been utilized for improving the sensitivity of conventional SiNW-FET sensors.

First, we carried out 2D process simulations and numerical simulations using ATHENA and ATLAS to investigate the electrical characteristics of an AM device^{20,21} (see supplementary material for further details²⁵). The channel implantation information to be used for the proper fabrication of an AM device was determined through the 2D process simulation, and the distribution of carriers in the bulk area within the NW was confirmed through both simulation and experiment. The fabrication process of the initial SiNW-FET (i.e., double-gate FinFET) is as follows. 8-in. silicon-on-insulator (SOI) *p*-type wafer with 100 nm of top silicon and 140 nm of buried oxide (BOX) was used as the starting material. As a first step, the top silicon was doped with boron at a doping level of $1 \times 10^{18}/\text{cm}^3$. Then, nitride with a thickness of 50 nm was deposited to serve as an etch stopper during the chemical-mechanical polishing (CMP) process that is carried out in a later step. Using optical lithography with a 193 nm wavelength of KrF followed by partial resist ashing and conventional plasma etching, the nanowire is patterned. Then, tetraethyl orthosilicate (TEOS) oxide with a thickness of 30 nm and n^+ *in situ* doped poly-crystalline silicon (poly-Si) with a thickness of 110 nm were deposited for the formation of the gate dielectric and the gate electrode. Through a subsequent CMP process, the connected single gate is separated

^{a)}Electronic mail: ykchoi@ee.kaist.ac.kr.

into two independent gates. Afterwards, the source and drain electrodes are formed through the implantation of arsenic at an energy level of 30 keV and a dose of $5 \times 10^{15}/\text{cm}^2$. The process explained thus far is for the n-channel IM-FET. For the fabrication of the AM-FET, a subsequent channel implantation, determined from the process simulation, was conducted with phosphorous at a dose of $6 \times 10^{13}/\text{cm}^2$ and energy level of 70 keV. The implantation was followed by rapid thermal anneal at 1000 °C for 10 s.

The configuration of the proposed device is illustrated in Fig. 1(a) (top-view). Through a slight modification of the aforementioned double-gate FinFET,²² where the silicon channel is sandwiched between two gate electrodes, the structure of the SiNW-FET sensor employed in this work is realized. As shown in Fig. 1(a), first, the initial gate oxide layer and the BOX layer underneath the NW are etched completely. Thus, with the removal of the BOX layer, the SiNW becomes suspended in air. Subsequently, 3 nm of thin oxide is thermally regrown on the exposed surfaces through re-oxidation. Finally, with the application of sufficient V_G , the NW attaches to one of the two gates. Figure 1(b) is the SEM image of the proposed device, and the cross-sectional view in Fig. 1(c) confirms the proper attachment of the NW onto the gate. The particular architecture of the device was realized mainly for two reasons: (1) to create a large air gap that can secure a safe immobilization of the biomolecules and (2) more importantly to obtain a single-gated SiNW structure in order to isolate the influence of two current components, bulk current, and surface current, during the analysis of the sensing properties of the devices. To elaborate more on the latter issue, the key to the enhanced sensitivity of AM-FETs is due to the current that flows in the bulk region as will be explained later. Thus, for a fair comparison of the AM and IM device, it is important that biomolecules are immobilized only on one side of the NW that is located at the opposite side of the active gate. Rather, if the biomolecules were to be immobilized on top of the NW where the nitride hard mask is currently located in Fig. 1(c), the biomolecules will affect both the surface current and the bulk current as biomolecules are oriented perpendicular to the gate. Therefore, such architecture is essential for the suggested study.

Figures 2(a) and 2(b) illustrate the electrical attachment, i.e., pull-in, of SiNWs onto the gate for AM and IM, respec-

tively. When the V_G reaches a certain voltage, the suspended SiNW suddenly adheres to the active gate, and the architecture takes the form of a single-gated SiNW-FET. When the device is read subsequently after the NW has been attached, the resulting current-voltage (I-V) characteristic is that of a metal-oxide semiconductor field-effect transistor (MOS-FET). During the pull-in operation, V_{DS} of 0.05 V was applied to the device. Due to this V_{DS} applied, as illustrated in Fig. 2(a), the current level for an AM device is already high even before the SiNW is attached to the gate. As the doping across the device is N^+-N-N^+ , the energy barrier between channel region and S/D is small, and thus V_{DS} is sufficient for the current to flow. As the SiNW is attached to the active gate, the gate capacitance is increased due to the larger gate dielectric. This accounts for the slight increase in the current level that can be seen in Fig. 2(a). After the pull-in, I-V curve shows that the device has transformed into a single-gated SiNW-FET. AM-FETs are normally-on devices and thus the current level is high at V_G of 0 V. To turn off the device, the bulk area of the NW must be pinched off by depletion. Therefore, to allow for the NW to be fully depleted, it is important that the NW width is narrow enough. As entire section of the NW is depleted, bulk current flowing at the middle of the NW is cut off. On the other hand, as can be seen in Fig. 2(b), for an IM-FET, no current can flow until the SiNW is fully attached to the gate. This is because an inversion channel cannot be formed due to the wide air gap that exists until pull-in occurs. After the pull-in, due to the sudden increase of the gate capacitance, inversion channel is formed and results in high current level. From Figs. 2(a) and 2(b), it can be noticed that although the conduction mechanism is different for AM and IM, apparently the two I-V curves are analogous to each other with the exception of threshold voltage (V_T) value.

The comparison of the biomolecule sensing properties of AM and IM devices was carried out using the binding of antibody and antigen of highly pathogenic avian influenza (AI) virus of influenza type A.²³ To help immobilize the AI surface antigen (AIa) on the NW, a silica-binding protein (SBP) was fused with AIa. Therefore, a fusion protein known as SBP-AIa was created, in which the SBP portion of the fusion protein serves as an anchor to the NW while AIa functions as the specific receptor molecule that binds with the

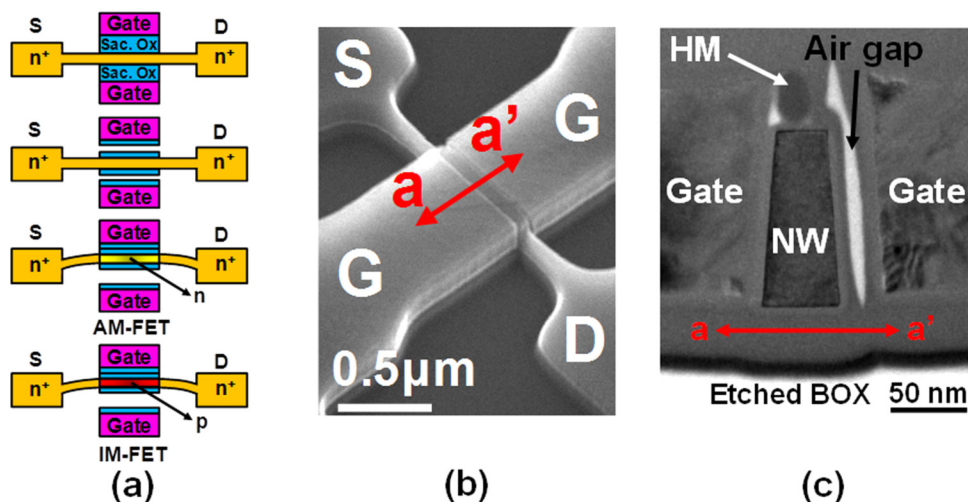


FIG. 1. (a) Schematic illustration of the proposed SiNW-FET sensors. From the initial double-gate FinFET, the final configuration is formed by an initial gate oxide removal (sacrificial oxide), followed by a slight re-oxidation, and finally the electrical attachment of the NW. Thus, a wide air gap is formed below the NW. AM device and IM device share the same structure and differ only in channel doping type. (b) Bird's eye view of the scanning electron microscope (SEM) image of the proposed device. (c) Cross-sectional transmission electron microscopy (TEM) image confirming the attachment of the NW onto the active gate.

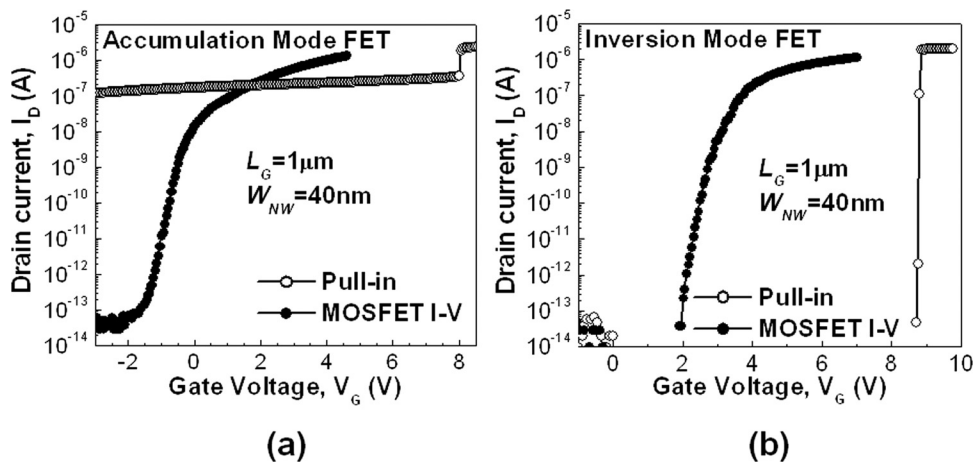


FIG. 2. The pull-in operation and the subsequent current-voltage (I-V) curve of the (a) AM device and (b) IM device. During the pull-in and the subsequent read of the single-gated SiNW FET, V_{DS} of 0.05 V and V_G were applied simultaneously.

antibody of AI (anti-AI). For the binding experiments, a drop of 100 μL of SBP-AIa dissolved in phosphate-buffered saline (PBS, pH 7.4) solution was cast on the devices for 1 h at room temperature. The devices were rinsed several times in de-ionized water and subsequently dried with N_2 gas. Then, anti-AI dissolved in PBS solution was dropped on devices immobilized with SBP-AIa for 1 h for the binding of antigen and antibody. While a fixed concentration of 25 $\mu\text{g}/\text{mL}$ (86.7 nmol/L) was used for SBP-AIa, various concentrations were used for anti-AI for the analysis of the device sensitivity.

The binding responses for AM and IM devices are represented in Figs. 3(a) and 3(b). When anti-AI molecules bind to SBP-AIa molecules that are immobilized on the NW surface, the net negative charge of anti-AI affects the electron density within the NW. In case for IM device, when the binding between anti-AI and SBP-AIa occurs, due to the electrochemical gating effect that arises from the extra negative charge introduced, the local electric potential in the channel

region is influenced. The negative charge coming from anti-AI mitigates the effect of V_G and therefore suppresses the formation of the inversion channel. Thus, the V_T is shifted towards the right. As for the AM device, as the device employed in this work is doped n-type, the negative charge of anti-AI causes depletion within the NW. As the negative charge of anti-AI causes extra depletion in addition to the effect of V_G , the NW becomes fully depleted at a less negative V_G , and therefore the V_T is shifted rightward.

When the response against the binding of antigen and anti-AI was examined with various anti-AI concentrations for AM and IM, the AM device exhibited much higher sensitivity. As illustrated in Fig. 4(a), while the lowest detectable concentration of anti-AI for IM device was 20 ng/mL (0.134 nmol/L), the AM device was able to detect down to 0.2 ng/mL (1.34 pmol/L). Below these values, the devices exhibited V_T shifts that are similar to the amount of V_T shift which occurred when only the buffer solution (i.e., PBS

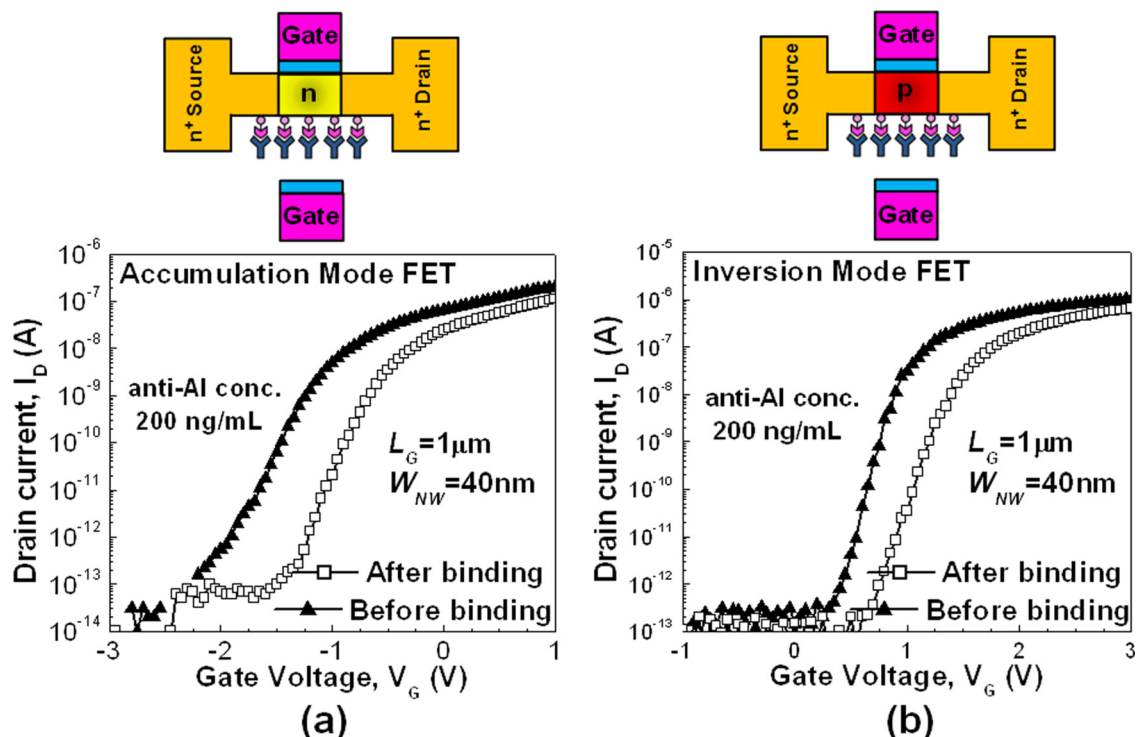


FIG. 3. I-V curves of the (a) AM device and (b) IM device before and after the binding of antigen and antibody of AI. For both devices, the V_T shifts rightward after the binding occurs. During the current reading, V_{DS} of 0.05 V was applied.

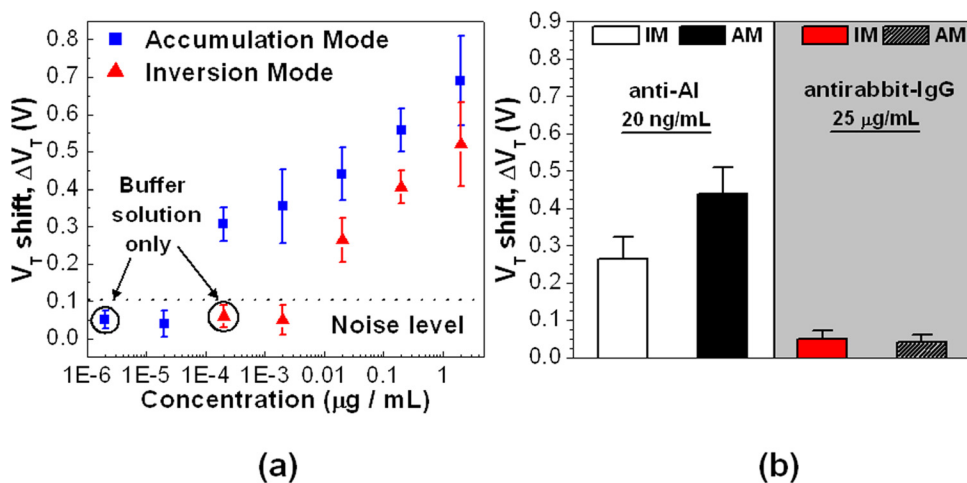


FIG. 4. (a) Comparison of the V_T shifts that occurred for AM and IM devices after binding. The horizontal axis represents the concentration of anti-AI, which had been dropped onto devices immobilized with SBP-AIa. The sensitivity of the IM device was enhanced by more than two orders (10^2) of magnitude when AM was employed. (b) Control experiment for specific binding with antirabbit-IgG.

solution) was used. Interestingly, in addition to the AM device showing far enhanced sensitivity, it also showed larger V_T shifts. Both outcomes are due to the different physics that account for the operation of AM-FETs. In an AM device, as mentioned above, current is not confined to the surface channel, and it consists of two components: surface current and bulk current. Therefore, in our case, when the biomolecules are attached to the bottom of the NW, the distance between the conduction path and the biomolecules is much closer for AM. In an earlier work, it had been demonstrated that the detection sensitivity of SiNW sensor relies highly on the relative distance between the NW surface and the charged biomolecule.²⁴ For IM devices, as current only flows through the inversion channel which is located at the surface area near the gate, current is farther away from the biomolecules. Therefore, when the concentration of the anti-AI is too small, the negative charge contained within anti-AI is insufficient to influence the electric potential within the surface channel. However, for an AM device, as the current flows through the entire NW, the negative charge does not necessarily need to directly affect the surface channel. Rather, by depleting the bottom portion of the NW, a significant amount of current can be blocked. To ensure the specificity of the proposed device, a control experiment was conducted with antirabbit immunoglobulins (antirabbit-IgG) as shown in Fig. 4(b). As expected, due to the non-specificity between SBP-AIa and antirabbit-IgG, the I-V characteristics showed negligible V_T shift which was almost equivalent in magnitude with the V_T shift that occurred when only the buffer solution was used.

In summary, with the employment of AM-FETs, we have shown that the device sensitivity can be enhanced exponentially compared with conventional IM-FETs. This result is attributed to the different underlying physics and conduction mechanism responsible for the AM device. The results have been verified in a direct comparison between the IM and AM devices under the same SiNW structure.

This work was supported by the Smart IT Convergence System Research Center funded by the Ministry of Education, Science and Technology as Global Frontier Project (SIRC-2011-0031845) and the National Research and Development Program (NRDP, 2012-0001131) for the development of biomedical function monitoring biosensors and the Technology Innovation Program through the Korea Innova-

tion Cluster Foundation funded by the Ministry of Knowledge Economy (A2010D-D013).

- ¹Y. Cui, Q. Wei, H. Park, and C. M. Lieber, *Science* **293**, 1289–1292 (2001).
- ²E. Stern, J. F. Klemic, D. A. Routenberg, P. N. Wyrembak, D. B. Turner-Evans, A. D. Hamilton, D. A. LaVan, T. M. Fahmy, and M. A. Reed, *Nature (London)* **445**, 519–522 (2007).
- ³Z. Fan and J. G. Lu, *Appl. Phys. Lett.* **86**, 123510 (2005).
- ⁴F. Patolsky and C. M. Lieber, *Mater. Today* **8**, 20–29 (2005).
- ⁵G. Zheng, F. Patolsky, Y. Cui, and C. M. Lieber, *Nat. Biotechnol.* **23**, 1294–1301 (2005).
- ⁶F. Patolsky, G. Zheng, and C. M. Lieber, *Anal. Chem.* **78**, 4260–4269 (2006).
- ⁷Y. Chen, X. Wang, S. Erramilli, and P. Mohanty, *Appl. Phys. Lett.* **89**, 223512 (2006).
- ⁸Z. Gao, A. Agarwal, A. D. Trigg, N. Singh, C. Fang, C. H. Tung, Y. Fan, K. D. Buddharaju, and J. Kong, *Anal. Chem.* **79**, 3291–3297 (2007).
- ⁹Z. Li, Y. Chen, X. Li, T. I. Kamins, K. Nauka, and R. S. Williams, *Nano Lett.* **4**, 245–247 (2004).
- ¹⁰J. A. Streifer, H. Kim, B. M. Nichols, and R. J. Hamers, *Nanotechnology* **16**, 1868–1873 (2005).
- ¹¹N. Elfstrom, R. Juhasz, I. Sychugov, T. Engfeldt, A. E. Karlstrom, and J. Linnros, *Nano Lett.* **7**, 2608–2612 (2007).
- ¹²C. Heitzinger and G. Klimeck, *J. Comput. Electron.* **6**, 387–390 (2007).
- ¹³P. R. Nair and M. A. Alam, *IEEE Trans. Electron Devices* **54**, 3400–3408 (2007).
- ¹⁴A. Kim, C. S. Ah, H. Y. Yu, J.-H. Yang, I.-B. Baek, C.-G. Ahn, C. W. Park, and M. S. Jun, *Appl. Phys. Lett.* **91**, 103901 (2007).
- ¹⁵X. P. A. Gao, G. Zheng, and C. M. Lieber, *Nano Lett.* **10**, 547–552 (2010).
- ¹⁶J.-P. Colinge, C.-W. Lee, A. Afzaljan, N. D. Akhavan, R. Yan, I. Ferain, P. Razavi, B. O'Neill, A. Blake, M. White, A.-M. Kelleher, B. McCarthy, and R. Murphy, *Nat. Nanotechnol.* **5**, 225–229 (2010).
- ¹⁷C.-W. Lee, A. Afzaljan, N. D. Akhavan, R. Yan, I. Ferain, and J.-P. Colinge, *Appl. Phys. Lett.* **94**, 053511 (2009).
- ¹⁸J. P. Duarte, S.-J. Choi, D.-I. Moon, and Y.-K. Choi, *IEEE Electron Device Lett.* **32**, 704–706 (2011).
- ¹⁹J. P. Duarte, S.-J. Choi, and Y.-K. Choi, *IEEE Trans. Electron Devices* **58**, 4219–4225 (2011).
- ²⁰*Athena User's Manual: 2D Process Simulation Software* (Silvaco Int., Santa Clara, CA, 2008).
- ²¹*Atlas User's Manual: Device Simulation Software* (Silvaco Int., Santa Clara, CA, 2008).
- ²²Y.-K. Choi, T.-J. King, and C. Hu, *IEEE Electron Device Lett.* **23**, 25–27 (2002).
- ²³B. Gu, T. J. Park, J.-H. Ahn, X.-J. Huang, S. Y. Lee, and Y.-K. Choi, *Small* **5**, 2407–2412 (2009).
- ²⁴G.-J. Zhang, G. Zhang, J. H. Chua, R.-E. Chee, E. H. Wong, A. Agarwal, K. D. Buddharaju, N. Singh, Z. Gao, and N. Balasubramanian, *Nano Lett.* **8**, 1066–1070 (2008).
- ²⁵See supplementary material at <http://dx.doi.org/10.1063/1.4723843> for simulation data consisting of 2-D process and numerical simulation that was conducted using ATHENA and ATLAS.